Human adipose stromal cells differentiate towards a tendon phenotype with adapted visco-elastic properties in a 3D-culture system

Maxime Hordé[a], Jonathan Fouchard[a], Xavier Laffray[b], Cédrine Blavet[a], Véronique Béréziat[c], Claire Lagathu[c], Ludovic Gaut [a], Delphine Duprez[a,1,#] and Emmanuelle Havis[a,1,#]

[a] Sorbonne Université, Institut Biologie Paris Seine, CNRS UMR7622, Developmental Biology Laboratory, Inserm U1156, F-75005 Paris, France

[b] Université Paris Est Creteil, Glycobiology, Cell Growth and Tissue Repair Research Unit (Gly-CRRET), EA 4397, F-94010 Creteil, France.

[c] Sorbonne Université, Inserm UMRS938, Centre de Recherche Saint-Antoine (CRSA), Institut Hospitalo-Universitaire de Cardio-Métabolisme et Nutrition (ICAN), F-75012 Paris, France

[1] Co-senior authors; [#] Co-corresponding authors

Key words: tendon differentiation program, tendon-associated matrix, viscoelastic properties, human adipose stromal cells, 3D-culture system

Abstract

Tendon cell differentiation relies on molecular and mechanical parameters that control the expression of tendon-associated transcription factors and extracellular matrix proteins. However, the minimal cues able to initiate tendon differentiation from progenitor cells remains unknown. We analysed the tendon differentiation program in human adipose stromal cells (hASCs) cultured in a minimal 3D-system. We generated 3D-hASC constructs by embedding hASCs in a type-I collagen gel under a static uniaxial geometrical constraint with no additional molecular and mechanical cues, and assessed tendon-associated gene expression and mechanical properties for up to three weeks in culture. Analysis of tendon-associated genes revealed a molecular progression consistent with the acquisition of a tendon phenotype. The analysis of viscoelastic properties of 3D-hASC constructs by nano-indentation indicated a progressive increase in tissue stiffness up to 10 kPa, concomitant with a reduced stress relaxation indicative of solid-like mechanical properties. These changes in mechanical properties parallel the molecular change of matrix genes during the time of cultures. In summary, we have established that hASCs cultured in a minimal 3D-system progress into the tendon differentiation program associated with variations of mechanical properties.

Introduction

Tendon cell differentiation relies on molecular and mechanical parameters, which are not fully identified. The minimal cues able to initiate the tendon differentiation program from stem cells remains unknown.

Tendon is a key component of the musculoskeletal system that transmits forces from muscle to bone to allow locomotion. To accomplish this function, tendons exhibit specific viscoelastic properties, with a Young's modulus much higher than other soft tissues (Peltonen et al. 2013; Connizzo and Grodzinsky 2017). Tendon is a connective tissue composed of tendon fibroblasts that produce a dense extracellular matrix (ECM) consisting mainly of type I collagen fibrils that display a specific spatial organisation to resist the tensile forces generated by muscle contraction. Compared to other components of the musculoskeletal system, little is known about the mechanisms involved in tendon cell differentiation from undifferentiated cells. There is no identified master gene for the tendon lineage. The tendon program is difficult to follow because of the lack of recognized markers for each step of the tendon differentiation program (Huang and Galloway 2023). There is no identified master gene driving the tendon program. Moreover, developmental tendon fibroblast populations are not well characterized and the molecular markers of tendon cell populations are not well identified (Hirsinger et al. 2024).

In vertebrates, type I collagen, encoded by *COL1A1* and *COL1A2* genes, is the main structural and functional component of tendons. The regulation of *COL1A1* transcription is under the control of several transcription factors at different steps of tendon formation. The main developmental tendon marker, the bHLH transcription factor Scleraxis (SCX) (Schweitzer et al. 2001) regulates *COL1A1* transcription during development (Murchison et al. 2007). Two other transcription factors have been shown to regulate *COL1A1* transcription in adult mouse tendons, EGR1 (Guerquin et al. 2013) and MKX (Mohawk) (Ito et al. 2010; Liu et al. 2010). In addition to *COL1A1* regulation, SCX is required and sufficient for the expression of the transmembrane glycoprotein *TNMD* (Tenomodulin) in developing limb tendons and tendon cell cultures (Shukunami et al. 2006; 2018; Murchison et al. 2007); TNMD being involved in tenocyte proliferation and tendon collagen fibril maturation in new-born mice (Docheva et al. 2005; Dex et al. 2017). This indicates that SCX acts as a starter of the tendon program, although not being a master gene for the tendon lineage. Tendons are still observed in *Scx* mutant mice; however, force-transmitting tendons display severe alterations with disorganized matrix (Murchison et al. 2007; Huang et al. 2019). The transcriptomic analysis of *SCX*-positive cells during mouse limb tendon development provided us with a list of genes enriched in fetal tendon

78 cells (Havis et al., 2014). Although the function of all the 100 top genes have not been studied,
79 when studied, gene function analyses show an involvement in tendon collagen fibrillogenesis;
80 exampled with *THBS2*, coding for Thrombospondin 2 a secreted ECM glycoprotein
81 (Kyriakides et al. 1998), *COL6A3* encoding the chainα3 of the non-fibrillar type VI collagen
82 (Pan et al. 2013) and *COL14A1* encoding the chainα1 of the FACIT (fibril-associated collagen
83 with interrupted triple helices) (Ansorge et al. 2009). Top 100 genes also include various ECM
84 proteins contributing to tendon biomechanical properties, such as the small leucine-rich
85 proteoglycan, DCN (Decorin) (Zhang et al. 2006), the secreted matrix protein POSTN
86 (Periostin) (Ackerman et al. 2024; Li et al. 2023), the collagen-bonding protein, DPT
87 (Dermatopontin) (Okamoto and Fujiwara 2006; de Micheli et al. 2020; Omoto et al. 2022) and
88 the lysyl oxidase enzyme LOX, which catalyzes collagens cross-linking of through oxidative
89 deamination of lysine residues (Nguyen et al. 2023). All these tendon-associated molecules
90 provide us with molecular markers to assess the developmental tendon phenotype. In addition
91 to molecular cues, mechanical parameters are key for tendon development. Axial, head and
92 limb tendon development is stopped in the absence of muscle contraction in chicken and mouse
93 models (Gaut and Duprez 2016; Havis et al. 2016).
94 Tendon cell differentiation is difficult to follow *in vitro*, since the tendon phenotype is
95 not maintained in tendon 2D-cell cultures. Stem cells require molecular stimuli to induce a
96 tendon phenotype when cultured in 2D (Otabe et al. 2015; Guerquin et al. 2013; Gaut et al.
97 2020). Compared to 2D-culture systems, 3D-culture systems are more favourable to trigger
98 tendon differentiation (Yang et al. 2013; Gaut et al. 2020; Jaiswal et al. 2020). Human, rat,
99 mouse and avian tendon fibroblasts have been extensively used in 3D-culture systems to study
100 collagen fibrillogenesis (Herchenhan et al. 2013; 2015; Kapacee et al. 2008; Avey, Valdez, and
101 Baar 2024; Bayer et al. 2010; Kalson et al. 2010). In a fibrin 3D-culture system, chicken
102 embryonic tendon cells were able to produce matrix genes resembling to native tendons (Yeung
103 et al. 2015).
104 Mesenchymal Stem Cells (MSCs) are a standard in the field of adult stem cell biology,
105 due to their high differentiation capacities in various cell lineages, including osteoblast,
106 adipocyte or chondrocyte. The use of MSC allows the study of the mechanisms by which the
107 tendon lineage is initially selected (Jaiswal et al. 2020). The tendon differentiation potential has
108 been analysed in numerous MSC types, such as bone marrow-derived Mesenchymal Stem Cells
109 (bmMSCs), human Adipose-derived Stromal Cells (hASCs), mouse MSCs (with the
110 C3H10T1/2 cell line). However, these 3D-culture systems made of MSCs require molecular
111 cues (Yang et al. 2013; Hsieh et al. 2018; Kapacee et al. 2010b; Guerquin et al. 2013; Gaut et

al. 2016) or mechanical loading (Scott et al. 2011; Pentzold and Wildemann 2022; Kuo and Tuan 2008; Guerquin et al. 2013; Park, Nazhat, and Rosenzweig 2022) to reach and maintain a tendon phenotype.

Here, we used a 3D-culture system with hASCs in a type I collagen hydrogel maintained between two anchor points to assess whether hASCs were able of undergoing a tendon differentiation program with no external molecular cues and mechanical stimulation for three weeks. The activation of tendon-associated gene expression (transcription factors, matrix and other tendon markers) combined with increased stiffness and reduced relaxation of 3D-hASC constructs show that hASCs are directed towards a tendon differentiation program. This shows that hASCs undergo towards a tendon phenotype in a minimal 3D-culture system with no external molecular or mechanical cues.

Results

Development of a minimal 3D-culture system with human Adipose Stromal Cells

Since adipose tissue is an attractive alternative source of MSCs (Zuk 2013; Kokai, Marra, and Rubin 2014), we chose hASCs isolated from the stromal vascular fraction of human adipose tissue collected after liposuction surgery (Béréziat et al. 2019; Gorwood et al. 2020) to analyze how MSC self-organize and differentiate when cultured in 3D-conditions. During embryonic development, tendon primordia are high-cell-density linear structures anchored between skeletal and muscle tissues. To mimic the tendon biophysical microenvironment, hASCs were homogenously embedded in a collagen hydrogel, which reproduces the native microenvironment of tendon tissues (Mousavizadeh et al. 2023; Garvin et al. 2003), deposited between two anchor points using the Flexcell technology (Supplementary Figure 1). This technology consists in a holder with 24 cylindrical moulds conferring a homogeneous and regular shape to the constructs. Each mould is perforated with vertical holes through which the vacuum is applied, allowing the silicon elastic surface of the well to acquire the shape of the mould (Fig.1A). At the extremities of each cylinder, two nylon anchor stems allowed the maintenance of static tension in each construct (Fig. 1A). After isolation and amplification, hASCs were embedded in a 3.5% bovine type I collagen solution and seeded between the two anchor stems. Vacuum was maintained for 2 hours to generate a construct of a cylindrical shape. 3D-hASC constructs (which we define as Day -2) were then left for 48 hours to allow cell development under static tension by condensing the surrounding matrix. 3D-constructs were analysed starting from this time point, defined as Day 0 (Fig. 1B). Once generated, the 3D-constructs were maintained under static conditions for 21 days (Fig. 1B). We did not apply external forces and the 3D-constructs were only subjected to the tension forces exerted between the two anchoring points. At Day 0, 3D-hASC constructs exhibited diameter values of 2.08+/-0.08 mm (Fig. 1D). The diameters of 3D-hASC constructs decreased drastically from Day 0 to Day 7 (0.67+/-0.02 mm at Day 7) and then displayed a slow decrease from Day 7 to Day 21 (0.59+/-0.02 mm at Day 14, 0.55+/-0.04 mm at Day 21) (Fig. 1D). Notably, because the length of the construct is fixed, we could estimate a volume reduction of 3D-constructs of about 15-fold in the course of the 21 Days of culture. 3D-no cell constructs not seeded with hASC exhibit constant diameter values during the 3 weeks of culture, 4.46+/- 0.48 mm at Day 0, 4.41+/-0.45 mm at Day 7, 4.5+/-0.45 mm at Day 14 and 4.46+/-0.48 mm at Day 21 (Supplementary Fig. 1D-E). Similarly, the cross-sectional areas of 3D-no cell constructs remain constant and significantly higher than those of 3D-hASC constructs (Supplementary Fig. 1F). The total

180 number of cells in the constructs remained relatively stable between Day 0 and Day 21, with a
181 slight increase at Day 7 and a slight decrease between Day 7 and Day 21 (Fig. 1D). We did not
182 observe any apoptosis features between Day 7 and Day 14 (Supplementary Fig. 2).
183 At a cellular level, hASCs in this 3D-culture system displayed a fusiform shape and
184 spindle-shaped nuclei, aligned in the direction defined by the two anchor points (Fig. 1E),
185 reminiscent of cell organisation in native tendons, while hASCs exhibited a star shape in 2D
186 cultures (Supplementary Fig. 1B). In addition, cells progressively aligned along the tension axis
187 as the angle between the cell axis and the axis of the 3D-hASC constructs decreased throughout
188 culture (Fig. 1F). RT-qPCR analysis of the expression of the main tendon collagen *COL1A1*
189 show a progressive increase from Day 0 to Day 21 (Fig. 1G). In situ hybridization revealed that
190 *COL1A1* was highly expressed in tendon constructs until Day 14 (Fig. 1H-I). However, at Day
191 21, *COL1A1* appeared to be more highly expressed in central cells than in ring cells (Fig. 1I).
192 We used this 3D-culture system to analyse the tendon differentiation potential of hASCs.
193
194 *hASCs are prone to tendon differentiation in a minimal 3D-culture system.*
195 In order to assess the tendon differentiation potential of hASCs cultured in the 3D-conditions
196 described above, we analysed tendon gene expression at the transcript levels with RT-qPCR
197 and in situ hybridization experiments. We started the analyse with recognized tendon markers
198 at different time points during the culture. The mRNA expression of the following genes was
199 first analysed: the recognized tendon markers *SCX*, *MKX*, *TNMD* and *THSB2*. *SCX* expression
200 was detected, although at low level, both by in situ hybridization and RT-qPCR (Fig. 2A-B).
201 *SCX* expression slightly increased up to Day 7, remained constant up to Day 14 and then
202 decreased up to Day 21 (Fig. 2A). *MKX* expression was not detected at Day 0 and Day 2, but
203 started to be expressed on Day 4 and increased up to Day 21 (Fig. 2C). Interestingly, *TNMD*
204 was expressed in all 3D-hASC constructs on Day 4 but was not detected or at low levels at the
205 other timepoints (Fig. 2D). *THBS2* mRNA expression was significantly increased during human
206 3D-hASCs construct development (Fig. 2E). We also analysed the expression of other genes
207 identified in the Top100 genes (ordered with the highest enrichment score) of *SCX*-positive
208 cells during mouse limb development (Havis et al., 2014), such as *TM4SF1* (Transmembrane 4
209 superfamily member 1, ranked 4th), *ANXA1* (Annexin A1, ranked 19th) and *S100A10* (member
210 of the S100 family of cytosolic Ca^{2+}-binding proteins, ranked 73rd). *TM4FS1* expression was
211 detected from Day 0 and increased significantly in 3D-hASC constructs overtime (Fig. 2G). In
212 contrast, *ANXA1* expression was first decreased at Day 2 and slightly increased at Day 21 (Fig.
213 2H). The *S100A10* expression levels were stable in 3D-hASC constructs until Day 14 and

214 slightly decreased between Day 14 and Day 21 (Fig. 2I). Consistent with the activation of the
215 tendon program, 3D-hASC constructs did not express osteogenic or adipogenic markers and
216 did not contain any adipocytes or osteocytes (Supplementary Fig. 3B-D). It has to be noted that
217 hASCs displayed the ability to differentiate into adipocytes and osteocytes in appropriate
218 culture media in 2D-culture conditions (Supplementary Fig. 3A-C) (Waldner et al. 2018; Kokai,
219 Marra, and Rubin 2014). The cartilage-specific collagen gene *COL2A1* was not detected 3D-
220 hASC constructs (Fig. 2J), indicating that hASCs had not differentiated into cartilage cells.
221 We conclude that hASCs undergo towards a tendon program when cultured in 3D-
222 conditions in a collagen gel maintained between two anchor points.
223
224 *The Young's modulus of 3D-hASC constructs increases over time.*
225 In order to assess whether the activation of the tendon program in hASCs was correlated with
226 a stiffening of the 3D-constructs, we measured the Young's modulus of 3D-hASC constructs
227 in the course of the 21 Days of culture. We used nanoindentation (Van Hoorn et al. 2016) to
228 probe the mechanical properties of the 3D-hASC constructs at the local scale (micron scale),
229 with the application of controlled deformations on the surface of the sample. To maintain the
230 3D-hASC constructs in an immobile position during the nanoindentation experiments, they
231 were detached from their anchor points and deposited onto a support composed of grooves
232 whose length and diameters were adjusted according to constructs geometry. The support was
233 maintained in a petri dish with agarose gel, while 3D-hASC constructs were fixed to the support
234 using dissection pins inserted through the anchor stems and in the agarose gel (Fig. 3A).
235 Indentation was performed by moving the base of the cantilever at a constant speed of $10 \mu m.s^{-}$
236 ^{1}, with beads of diameters ranged from 50 to 100 µm (Fig. 3B-D). The relationship between
237 applied force and deformation provides information about 3D-hASCs construct mechanical
238 properties. In particular, tissue effective Young's modulus E_{eff} was calculated by fitting the
239 force-indentation curve over a one-micron indentation range using the Hertz model (Fig. 3E,
240 see methods). The effective Young's modulus increased significantly during the 21 Days of
241 construct culture starting from 1.3 kPa at Day 0 to 9.2 kPa at Day 21 (Fig. 3F). Notably, E_{eff}
242 increased by two-fold factor every seven days. The effective Young's modulus of 3D-
243 constructs not seeded with cells remains constant for 21 days, at 0.4 kPa (Fig. 3G).
244 We conclude that 3D-hASC constructs display an increased stiffness over time.
245
246

247 *Extracellular matrix gene expression is correlated with changes in viscoelastic properties of*
248 *3D-hASC constructs.*
249 Tendon stiffness relies on the synthesis of a dense and organized extracellular matrix generated
250 by tendon cells. We thus analysed the expression of transcripts encoding tendon-associated
251 collagens and fibrillogenesis-associated proteins during 3D-hASC constructs formation.
252 Similarly to *COL1A1* (Fig. 1G), the mRNA levels of the tendon-associated collagens *COL6A3*
253 and *COL14A1* were detected at Day 0, increased until Day 7 and remained higher at Day 21
254 compared to Day 0 (Fig. 4A-B). We also analysed the expression of genes encoding
255 fibrillogenesis-associated proteins, *DPT*, *DCN*, *POSTN* and *LOX* which exhibit an elevated
256 enrichment score in E14.5 compared to E11.5 *SCX*-positive cells during mouse limb
257 development (Havis et al., 2014). The transcript levels of *DPT*, *DCN*, *POSTN* and *LOX* were
258 significantly increased during human 3D-hASC construct formation (Fig. 4C-F). The persistent
259 increase of tendon collagen and collagen fibrillogenesis gene expression was indicative of
260 matrix production and parallel the increase of effective Young's modulus (Fig. 3F) during 3D-
261 hASCs construct formation. In addition, the increased expression of *DPT*, *DCN*, *POSTN*,
262 *THBS2* and *LOX*, regulators of ECM network, also suggested that the structure and organisation
263 of the ECM was modified during the course of 3D-hASC construct formation. We thus tested
264 whether ECM transcript expression was accompanied with a modification of the viscoelastic
265 properties of 3D-hASC constructs along time. To do this, we carried out stress relaxation
266 experiments using nanoindentation (Fig. 5). In particular, we calculated the percentage of
267 relaxation r_{relax} from the peak force F_{max} measured at the end of the indentation ramp and the
268 force $F_{t=10s}$ measured after 10 seconds of relaxation ($r_{relax} = (F_{max}-F_{t=10s})/F_{max}$). The higher this
269 ratio is, the more liquid-like the material. Oppositely, a smaller ratio indicates more solid,
270 elastic-like viscoelastic properties. On Day 0, the percentage of relaxation of 3D-hASCs was
271 35% and decreased along time down to 24% on Day 21 (Fig. 5E), in parallel with the increase
272 of ECM transcript levels. Interestingly, the percentage of relaxation of 3D-no cell constructs on
273 Day 0 was 23%, decreased to 15% on Day 7 and remained constant (Fig. 5E).
274 We conclude that the 3D-hASC constructs acquire solid-like properties, consistent with
275 the expression of matrix transcripts during the time course of the cultures.
276
277 *3D-hASC constructs organize into two cell populations.*
278 In order to analyse cell organisation, we performed longitudinal and transverse sections of 3D-
279 hASC constructs (Fig. 1E, Supplementary Fig. 4, Fig. 6). We identified two cell populations,
280 one at the centre and the other one at the periphery as a ring, as soon as Day 2 (Fig. 6B).

Phalloidin staining showed that the peripheral cell population formed a ring composed of 3 to 4 cell layers from Day 4 to Day 21, which was separated from the central region by a sharp interface (Fig. 6B). Cell density at the ring and the centre was maintained from Day 4 to Day 21 (Fig. 6C). Interestingly, the expression of ECM genes evolved in the two cell populations in a different manner (Fig. 1I, 2F). *COL1A1* was expressed in both centre and ring cells of 3D-hASC constructs with in situ hybridization from Day 7 to Day 14 (Fig. 1I). However, at Day 21, *COL1A1* displayed stronger expression in centre cells compared to ring cells (Fig. 1I). By contrast, *THBS2* was visualized in both centre and ring 3D-hASCs construct cells along the 21 days of culture (Fig. 2F). In addition, a marker of peripheral cells of adult rat tendons *COL3A1* (Steffen, Mienaltowski, and Baar 2023) was detected both in centre and ring cells of 3D-hASC constructs, suggesting that the cells at the periphery were not mature peritenon cells (Supplementary Fig. 5).

We conclude that 3D-hASC constructs self-organize into cell populations with different location.

Discussion

This study showed that hASCs enter the tendon differentiation program when cultured in a minimal 3D-system. hASCs embedded into a cylindrical scaffold of type I-collagen attached to two anchor points acquired stiffness and solid-like properties that parallel the expression of tendon matrix genes.

The genetic program activated in 3D-hASCs mimics that of tendon development.

With no external molecular cues other than the culture medium, hASCs mixed in a 3D-collagen gel expressed tendon genes encoding transcription factors regulating *COL1A1* transcription and tendon matrix genes. The molecular progression in 3D-hASCs is reminiscent of tendon gene expression during development. *SCX* and *MKX* are sequentially expressed in 3D-hASC constructs, as during mouse tendon development (Liu et al. 2010; Ito et al. 2010). The expression pattern of *SCX* displays a bell shape, while the tendon matrix gene expression increases overtime in 3D-hASC constructs, consistent with SCX function as a starter of the developmental tendon program. The sequential expression of *SCX* and *TNMD* and the decrease of *SCX* and *TNMD* at Day 21 in the 3D-hASC constructs are consistent with *TNMD* regulation by SCX (Shukunami et al. 2018; Murchison et al. 2007). The two newly-identified genes, *TM4SF1* and *ANXA1,* coding for a Tetraspanin transmembrane protein and AnnexinA1, respectively, display a regular increase overtime as the *LOX* gene (lysyl oxidase proteins). Interestingly, the *TM4SF1*, *ANXA1* and *LOX* genes have been identified in a fibroblast cluster for good prognosis in bladder cancer (J. Wang et al. 2024) and are seen as therapeutic targets for fibrosis (Yan et al. 2022; Chen, Li, and Li 2019; Zhao et al. 2024). ANXA1 and S100A10 belong to two families of proteins known to form hetero-tetramers (Réty et al. 2000), suggesting that ANXA1 interacts with S100A10 to maintain the tendon phenotype of 3D-hASC constructs. The mRNA expression levels of the tendon-associated collagen genes (*COL1A1*, *COL6A3*, *COL14A1)* and genes encoding proteins involved in tendon collagen fibrillogenesis (*THBS2*, *DCN, POSTN, DPT)* rise sharply during the formation of 3D-hASC constructs, and were maintained at high levels at the end of culture. These results indicate that the reduced expression of *SCX* in 3D-hASCs does not affect the molecular identity of tendon ECM in the constructs.

349 *Progression of mechanical properties of hASCs in 3D-cultures*

350 During the 21-day culture period, the 3D-hASCs showed reduced diameter, increased stiffness
351 and reduced relaxation. The reduction in the diameter of 3D-hASC constructs was already
352 observed in 3D-constructs using human dermal fibroblasts (HDF01035) or calf patellar tendon
353 cells embedded in a collagen gel (Schulz Torres et al. 2000; Vaughan et al. 2019). Because the
354 diameters of 3D-constructs without any cell remained constant, we conclude that hASCs were
355 responsible for the collagen compaction of 3D-hASC constructs.

356 There is a linear increase of the stiffness of 3D-hASC constructs during the time of
357 culture. Notably, E_{eff} increased by two-fold factor every seven days. This indicates that this
358 long time-scale stiffening is unlikely to be due to ECM compaction, which occurred almost
359 exclusively during the first week of culture. We rather believe that the expression of genes
360 encoding specific ECM components would drive collagen compaction. After three weeks of
361 cell culture, 3D-hASC constructs exhibited a Young's modulus values comprised between 5.6
362 and 18.3 kPa. Interestingly, measurements of nanoscale elastic modulus of chicken foetal
363 calcaneus tendons calculated similarly through Hertz contact theory gave results of same order
364 of magnitude (5-17 kPa) (Marturano et al. 2013; Connizzo and Grodzinsky 2017). This suggests
365 that 3D-hASC constructs mimic the progression of mechanical properties observed during
366 tendon development. In studies using human adult tendon fibroblasts (not MSCs) to generate
367 3D constructs, Young's modulus measurements lead to a value close to that found by tensile
368 tests in adult tendons, of the order of MPa (Avey, Valdez, and Baar 2024; Herchenhan et al.
369 2013).

370

371 *Link between matrix gene expression and mechanics in 3D-hASC constructs*

372 The increase of expression of ECM-encoding genes parallels the stiffness increase and
373 concomitant relaxation reduction of 3D-hASC constructs. We see this correlation as a
374 bidirectional interaction between mechanical properties and matrix components during the time
375 of the culture. It is recognized that changes of physical properties act on matrix composition
376 and conversely, matrix interferes with mechanical properties (Saraswathibhatla, Indana, and
377 Chaudhuri 2023). We found that hASCs progressively acquired a spindle-shaped form
378 associated with elongation of the cell shape during the course of the 3D-culture, as observed in
379 native tendons. The elongated shape of cells observed in native tendons and 3D-hASC
380 constructs is probably involved in tendon matrix production, since nuclear response upon
381 deformation is recognized to include changes in transcriptional activity (Miroshnikova and
382 Wickström 2022).

3D-hASC constructs self-organize into two cell populations, one being at the centre of the construct and the other forming a ring at the periphery. Such organisation has been previously described in 3D-constructs generated with the Flexcell technology either with hASCs (Yang et al. 2013) or avian tendon internal fibroblasts (Garvin et al. 2003). This cell organisation may be an effect of the geometry of the constructions defined by the anchoring points, which may orient cell shape and ECM. The peripheral cells layer of 3D-hASC constructs is reminiscent of the peritenon external layer surrounding native tendon. This is consistent with the lower *COL1A1* expression in the ring cells compared to centre cells in 3D-hASC constructs at Day 21 (Fig. 1I), also observed in equine and rat peritenon cells versus tendon core cells (Pechanec et al. 2020; Steffen, Mienaltowski, and Baar 2023). *COL3A1* was identified recently as a peritenon marker in adult rat patellar tendons (Steffen, Mienaltowski, and Baar 2023). However, *COL3A1* was detected both at the centre and the periphery of 3D-hASC constructs (Supplementary Fig. 5), indicating that *COL31A1* expression does not discriminate the peritenon identity between ring and centre cells in 3D-hASC constructs. Interestingly, a peripheral layer has been identified surrounding developing tendons in mouse and chicken embryos (Eloy-Trinquet et al., 2009; Havis et al., 2014; Hirsinger et al., 2024), indicating that future peritenon cells are present early during the tendon program.

Although the 3D-hASC constructs display a tendon matrisome gene expression profile at 3 weeks, we do not exclude that external mechanical cues would improve the tendon phenotype of 3D-hASC constructs as already reported (Park, Nazhat, and Rosenzweig 2022; T. Wang et al. 2018). During development, muscle contractions are recognized to maintain *SCX* expression and the tendon phenotype in developing tendons (Gaut and Duprez 2016). An interesting hypothesis is that application of external mechanical cues would prevent *SCX* and *TNDM* down-regulation in 21-day-old 3D-hASC constructs.

In summary, we have established that hASCs, cultured in a minimal 3D-system progress into the tendon differentiation program along three weeks of culture. The molecular tendon program is associated with variations of mechanical properties reminiscent of embryonic tendon development.

Experimental procedures

Cell sample collection

Human abdominal subcutaneous adipose tissues were obtained from healthy donors after liposuction surgery (AP-HP Saint-Antoine Hospital, Paris, France). Human Adipose stromal cells (hASCs) were isolated from 3 healthy donors (one woman and two men).

All donors provided their written, informed consent to the use of their tissue specimens for research purposes. The study was performed in compliance with the principles of the Declaration of Helsinki and was approved by an institutional review board. The study was approved by the French regulatory authorities (Codecoh DC2023-5617). Cells were cryopreserved in 2mL cryotubes (2x106 cells per vial) stored in liquid nitrogen tanks.

Cell amplification

For each experiments, cell vials were thawed 2-3 min in a 37°C water bath and transferred in T25 cell culture flasks (Gibco) with 5ml of hASCs culture medium containing Minimum Essential Mediun (αMEM; Gibco; ref 22571-020) complemented with 10% Fetal Calf Serum (FCS; Gibco; ref 35-079-CV), 1% HEPES (1M, sigma; ref H0887-100ml), 1% glutamine (100X, 200mM, Gibco; ref 25030-024), 1% Penicillin/Streptomycin (Gibco; ref 15140-122) and 2.5 ng/mL FGF2 (PeproTech, Rocky Hill, NJ; ref 100-18B). Confluent cells were submitted to 2 passages, at 1:9 and 1:3 ratio. For each passage, we used 0.05% Trypsin (Gibco; ref 25300-054) for 5 minutes.

Preparation of 3D-hASC constructs

3D-hASC constructs were prepared as described (Scott et al. 2011). Briefly, sub confluent cells were detached in 5 ml of 0.05% trypsin for 5 minutes, then suspended with hASC culture medium (described below) and counted with a Malassez counting chamber. 16.2 million cells (600,000 cells per 3D-hASC construct) were centrifuged at 1200 rpm for 5 minutes and resuspended in 4.05 mL of Type I collagen solution containing 70% Purecoll (Sigma-Aldritch, Oakville, Canada; ref 5074-35ml), 10% FCS and 20% αMEM brought to 7.4 pH with 0.1 N NaOH immediately before use. 150 µl of hASCs-collagen mix was pipetted into each well of an untreated TissueTrain© plate (FlexCell International, Hillsborough NC; ref TTLC-4001C) according to the manufacturer's instructions. The collagen hydrogel was allowed to set for 2 hours, and the 3D-hASC constructs were covered with 2 ml of hASC culture medium completed with 0.25 mM ascorbic acid. The medium was replaced every 2-3 Days.

451 *3D-hASC construct sections*

452 3D-hASC constructs were fixed in 1% paraformaldehyde (PFA, Gibco Sigma; ref 158127-
453 100G) overnight at 4°C, washed in 1X PBS (Gibco; ref :14190-094) and put in a 15% sucrose
454 solution at 4°C for 3 Days. Before inclusion, 3D-hASC constructs were incubated in a 7,5%
455 gelatin-15% sucrose solution in a 37°C water bath for 1 hour. Included 3D-hASC constructs
456 were then frozen at -80°C in isopentane for 1 minute and 12µm longitudinal and transversal
457 cryosections were generated with a CM3050 S Cryostat (Leica Biosystems).

458

459 *Cell angle measurements*

460 Longitudinal sections were stained with DAPI (D9542, Sigma-Aldrich) to visualize cell nuclei
461 and phalloidin (A12380 Alexa Fluor Phalloidin, Invitrogen/ ThermoFisher scientific) to
462 visualize cytoskeletal F-actin. Fluorescent images were captured using a Zeiss Axio Observer
463 Z1 microscope equipped with a Zeiss Apotome 2 and an Axiocam 506 monochrome camera.
464 Cell/nucleus angles relative to the axis of the 3D-hASC constructs were measured using Fiji
465 Image J software.

466

467 *RNA isolation*

468 Entire 3D-hASC constructs were put in 500µL RLT (Qiagen; ref 74106) and homogenized
469 using a mechanical disruption device (Lysing Matrix A, Fast Prep MP1, 4 × 30 s, 6 $m.s^{-1}$). Total
470 RNA was isolated using the RNeasy mini kit (Qiagen; ref 74106), according to the
471 manufacturer's instructions, including a 15 min of DNase I (Qiagen; ref 79254) treatment.

472

473 *Reverse-Transcription and quantitative real time PCR*

474 500ng of total RNAs extracted from each 3D-hASCs construct, for each timepoint, were
475 Reverse Transcribed using the High Capacity Retro-transcription kit (Applied Biosystems; ref
476 4387406). Quantitative PCR analyses were performed using primers listed in Supplementary
477 Table 1 and SYBR Green PCR Master Mix (Applied Biosystems; ref 4385614). The relative
478 mRNA levels were calculated using the $2^{-\Delta\Delta Ct}$ method (Livak and Schmittgen 2001). The cycle
479 threshold (C_T) corresponds to the number of cycles required for the fluorescent signal to cross
480 the threshold (to exceed background level). The ΔC_Ts were obtained from C_T normalized to
481 *YWHAZ* C_T level in each sample. The primers used for RT-qPCR experiments are listed in
482 Supplementary table 1.

483

484

In situ hybridization

3D-hASCs construct 12µm cryosections were subject to a standard in situ hybridization protocol (Bonnin et al. 2005). *COL1A1, SCX, THBS2 and COL3A1* and probes were generated using a Roboprobe kit (Promega; ref P1460), according to manufacturer's instructions. Images were captured using a Nanozoomer SQ Digital Slide Scanner with NDP.view2 software (Hamamatsu Photonics). The primers used for probe synthesis are listed in Supplementary table 1.

Nanoindentation measurements

Live 3D-hASC constructs were detached from their anchor points and immediately fixed onto a 3D-printed support. To avoid sliding of the construct during mechanical testing, the support was designed with three half-cylindrical grooves at its surface whose diameters were adjusted to the typical 3D-hASC constructs diameters. In order to conserve the original length of the 3D-hASCs construct, the length of the support was also calibrated to the original distance between the anchor points in the bioreactor. The support was then embedded in an agarose gel in a Petri dish, and the samples were immersed in culture medium. Mechanical testing was performed at room temperature, using a Piuma nano-indenter (Optics11 Life), as described in the main text. Samples were positioned under the probe using a magnifying glass. Five measurements were performed along the 3D-hASCs construct length and their mean value was calculated to extract effective Young's modulus and percentage of stress relaxation for each sample.

The effective Young's modulus E_{eff} was calculated from a fit of the force versus indentation curve over a 1µm indentation course and using a Hertzian contact model as follows:

$$F = \frac{4}{3} E_{eff} \sqrt{R_i} \cdot h^{3/2}$$

where F is the force, Ri the tip radius, and h the indentation.

Statistical analyses

Data was analysed using the non-parametric Mann-Whitney test with Graphpad Prism V10. Results are shown as means ± standard deviations. The p-values are indicated either with the value or with * or #.

Funding sources

This work was supported by the CNRS, INSERM, Sorbonne University and ANR_TENORS.

Acknowledgements

We would like to thank Mathieu Hautefeuille for proofreading the manuscript.

References

Ackerman, Jessica E., Samantha N. Muscat, Emmanuela Adjei-Sowah, Antonion Korcari, Anne E.C. Nichols, Mark R. Buckley, and Alayna E. Loiselle. 2024. 'Identification of Periostin as a Critical Niche for Myofibroblast Dynamics and Fibrosis during Tendon Healing'. *Matrix Biology* 125 (January):59–72. https://doi.org/10.1016/j.matbio.2023.12.004.

Ansorge, Heather L., Xianmin Meng, Guiyun Zhang, Guido Veit, Mei Sun, John F. Klement, David P. Beason, Louis J. Soslowsky, Manuel Koch, and David E. Birk. 2009. 'Type XIV Collagen Regulates Fibrillogenesis: Premature Collagen Fibril Growth and Tissue Dysfunction in Null Mice'. *Journal of Biological Chemistry* 284 (13): 8427–38. https://doi.org/10.1074/jbc.M805582200.

Avey, Alec M., Omar Valdez, and Keith Baar. 2024. 'Characterization of an in Vitro Engineered Ligament Model'. *Matrix Biology Plus* 21 (February). https://doi.org/10.1016/j.mbplus.2023.100140.

Bayer, Monika L., Chin Yan C. Yeung, Karl E. Kadler, Klaus Qvortrup, Keith Baar, René B. Svensson, S. Peter Magnusson, Michael Krogsgaard, Manuel Koch, and Michael Kjaer. 2010. 'The Initiation of Embryonic-like Collagen Fibrillogenesis by Adult Human Tendon Fibroblasts When Cultured under Tension'. *Biomaterials* 31 (18): 4889–97. https://doi.org/10.1016/j.biomaterials.2010.02.062.

Béréziat, Véronique, Christelle Mazurier, Martine Auclair, Nathalie Ferrand, Séverine Jolly, Tiffany Marie, Ladan Kobari, et al. 2019. 'Systemic Dysfunction of Osteoblast Differentiation in Adipose-Derived Stem Cells from Patients with Multiple Myeloma'. *Cells* 8 (5): 1–16. https://doi.org/10.3390/cells8050441.

Bonnin, Marie Ange, Christine Laclef, Régis Blaise, Sophie Eloy-Trinquet, Frédéric Relaix, Pascal Maire, and Delphine Duprez. 2005. 'Six1 Is Not Involved in Limb Tendon Development, but Is Expressed in Limb Connective Tissue under Shh Regulation'. *Mechanisms of Development* 122 (4): 573–85. https://doi.org/10.1016/j.mod.2004.11.005.

Chen, Lijun, Shifeng Li, and Wande Li. 2019. 'LOX/LOXL in Pulmonary Fibrosis: Potential Therapeutic Targets'. *Journal of Drug Targeting* 27 (7): 790–96. https://doi.org/10.1080/1061186X.2018.1550649.

Connizzo, Brianne K., and Alan J. Grodzinsky. 2017. 'Tendon Exhibits Complex Poroelastic Behavior at the Nanoscale as Revealed by High-Frequency AFM-Based Rheology'. *Journal of Biomechanics* 54:11–18. https://doi.org/10.1016/j.jbiomech.2017.01.029.

Dex, Sarah, Paolo Alberton, Lena Willkomm, Thomas Söllradl, Sandra Bago, Stefan Milz, Mehdi Shakibaei, et al. 2017. 'Tenomodulin Is Required for Tendon Endurance Running

563 and Collagen I Fibril Adaptation to Mechanical Load'. *EBioMedicine* 20 (June):240–54.
564 https://doi.org/10.1016/j.ebiom.2017.05.003.
565 Docheva, Denitsa, Ernst B Hunziker, Reinhard Fässler, and Oliver Brandau. 2005.
566 'Tenomodulin Is Necessary for Tenocyte Proliferation and Tendon Maturation'.
567 *Molecular and Cellular Biology* 25 (2): 699–705.
568 https://doi.org/10.1128/MCB.25.2.699-705.2005.
569 Eloy-Trinquet, Sophie, Hui Wang, Fréderic Edom-Vovard, and Delphine Duprez. 2009. 'Fgf
570 Signaling Components Are Associated with Muscles and Tendons during Limb
571 Development'. *Developmental Dynamics* 238 (5): 1195–1206.
572 https://doi.org/https://doi.org/10.1002/dvdy.21946.
573 Garvin, Joanne, Jie Qi, Melissa Maloney, and Albert J. Banes. 2003. 'Novel System for
574 Engineering Bioartificial Tendons and Application of Mechanical Load'. *Tissue*
575 *Engineering* 9 (5): 967–79. https://doi.org/10.1089/107632703322495619.
576 Gaut, Ludovic, Marie Ange Bonnin, Ceìdrine Blavet, Isabelle Cacciapuoti, Monika Orpel,
577 Mathias Mericskay, and Delphine Duprez. 2020. 'Mechanical and Molecular Parameters
578 That Influence the Tendon Differentiation Potential of C3H10T1/2 Cells in 2D- And 3D-
579 Culture Systems'. *Biology Open* 9 (2). https://doi.org/10.1242/bio.047928.
580 Gaut, Ludovic, and Delphine Duprez. 2016. 'Tendon Development and Diseases'. *Wiley*
581 *Interdisciplinary Reviews: Developmental Biology* 5 (1): 5–23.
582 https://doi.org/10.1002/wdev.201.
583 Gaut, Ludovic, Nicolas Robert, Antony Delalande, Marie Ange Bonnin, Chantal Pichon, and
584 Delphine Duprez. 2016. 'EGR1 Regulates Transcription Downstream of Mechanical
585 Signals during Tendon Formation and Healing'. *PLoS ONE* 11 (11): 1–16.
586 https://doi.org/10.1371/journal.pone.0166237.
587 Gorwood, Jennifer, Tina Ejlalmanesh, Christine Bourgeois, Matthieu Mantecon, Cindy Rose,
588 Michael Atlan, Delphine Desjardins, et al. 2020. 'SIV Infection and the HIV Proteins Tat
589 and Nef Induce Senescence in Adipose Tissue and Human Adipose Stem Cells,
590 Resulting in Adipocyte Dysfunction'. *Cells* 9 (4). https://doi.org/10.3390/cells9040854.
591 Guerquin, M.-J., B. Charvet, G. Nourissat, E. Havis, O. Ronsin, M.-A. Bonnin, M. Ruggiu, et
592 al. 2013. 'Transcription Factor EGR1 Directs Tendon Differentiation and Promotes
593 Tendon Repair'. *Journal of Clinical Investigation* 123 (8).
594 https://doi.org/10.1172/JCI67521.
595 Havis, E., M.-A. Bonnin, I. Olivera-Martinez, N. Nazaret, M. Ruggiu, J. Weibel, C. Durand,
596 et al. 2014. 'Transcriptomic Analysis of Mouse Limb Tendon Cells during
597 Development'. *Development (Cambridge)* 141 (19). https://doi.org/10.1242/dev.108654.
598 Havis, Emmanuelle, Marie-Ange Bonnin, Joana Esteves de Lima, Benjamin Charvet, Cécile
599 Milet, and Delphine Duprez. 2016. 'TGFβ and FGF Promote Tendon Progenitor Fate
600 and Act Downstream of Muscle Contraction to Regulate Tendon Differentiation during
601 Chick Limb Development'. *Development* 143 (20): 3839–51.
602 https://doi.org/10.1242/dev.136242.
603 Havis, Emmanuelle, Marie-Ange Bonnin, Isabel Olivera-Martinez, Nicolas Nazaret, Mathilde
604 Ruggiu, Jennifer Weibel, Charles Durand, et al. 2014. 'Transcriptomic Analysis of
605 Mouse Limb Tendon Cells during Development'. *Development* 141 (19): 3683–96.
606 https://doi.org/10.1242/dev.108654.
607 Herchenhan, Andreas, Monika L. Bayer, René B. Svensson, S. Peter Magnusson, and Michael
608 Kjær. 2013. 'In Vitro Tendon Tissue Development from Human Fibroblasts
609 Demonstrates Collagen Fibril Diameter Growth Associated with a Rise in Mechanical
610 Strength'. *Developmental Dynamics* 242 (1): 2–8. https://doi.org/10.1002/dvdy.23896.
611 Herchenhan, Andreas, Franziska Uhlenbrock, Pernilla Eliasson, Maryann Weis, David Eyre,
612 Karl E. Kadler, S. Peter Magnusson, and Michael Kjaer. 2015. 'Lysyl Oxidase Activity

Is Required for Ordered Collagen Fibrillogenesis by Tendon Cells'. *Journal of Biological Chemistry* 290 (26): 16440–50. https://doi.org/10.1074/jbc.M115.641670.

Hirsinger, Estelle, Cédrine Blavet, Marie Ange Bonnin, Léa Bellenger, Tarek Gharsalli, and Delphine Duprez. 2024. 'Limb Connective Tissue Is Organized in a Continuum of Promiscuous Fibroblast Identities during Development'. *IScience* 27 (7). https://doi.org/10.1016/j.isci.2024.110305.

Hoorn, Hedde Van, Nicholas A. Kurniawan, Gijsje H. Koenderink, and Davide Iannuzzi. 2016. 'Local Dynamic Mechanical Analysis for Heterogeneous Soft Matter Using Ferrule-Top Indentation'. *Soft Matter* 12 (12): 3066–73. https://doi.org/10.1039/c6sm00300a.

Hsieh, Chi Fen, Zexing Yan, Ricarda G. Schumann, Stefan Milz, Christian G. Pfeifer, Matthias Schieker, and Denitsa Docheva. 2018. 'In Vitro Comparison of 2D-Cell Culture and 3D-Cell Sheets of Scleraxis-Programmed Bone Marrow Derived Mesenchymal Stem Cells to Primary Tendon Stem/Progenitor Cells for Tendon Repair'. *International Journal of Molecular Sciences* 19 (8). https://doi.org/10.3390/ijms19082272.

Huang, Alice H., and Jenna L. Galloway. 2023. 'Current and Emerging Technologies for Defining and Validating Tendon Cell Fate'. *Journal of Orthopaedic Research* 41 (10): 2082–92. https://doi.org/10.1002/jor.25632.

Huang, Alice H, Spencer S Watson, Lingyan Wang, Brendon M Baker, Haruhiko Akiyama, John V Brigande, and Ronen Schweitzer. 2019. 'Requirement for Scleraxis in the Recruitment of Mesenchymal Progenitors during Embryonic Tendon Elongation'. *Development* 146 (20): dev182782. https://doi.org/10.1242/dev.182782.

Ito, Yoshiaki, Naoya Toriuchi, Teruhito Yoshitaka, Hiroe Ueno-Kudoh, Tempei Sato, Shigetoshi Yokoyama, Keiichiro Nishida, et al. 2010. 'The Mohawk Homeobox Gene Is a Critical Regulator of Tendon Differentiation'. *Proceedings of the National Academy of Sciences of the United States of America* 107 (23): 10538–42. https://doi.org/10.1073/pnas.1000525107.

Jaiswal, Devina, Laurie Yousman, Maxwell Neary, Emily Fernschild, Brennen Zolnoski, Sara Katebifar, Swetha Rudraiah, Augustus D. Mazzocca, and Sangamesh G. Kumbar. 2020. 'Tendon Tissue Engineering: Biomechanical Considerations'. *Biomedical Materials (Bristol)* 15 (5). https://doi.org/10.1088/1748-605X/ab852f.

Kalson, Nicholas S., David F. Holmes, Zoher Kapacee, Iker Otermin, Yinhui Lu, Roland A. Ennos, Elizabeth G. Canty-Laird, and Karl E. Kadler. 2010. 'An Experimental Model for Studying the Biomechanics of Embryonic Tendon: Evidence That the Development of Mechanical Properties Depends on the Actinomyosin Machinery'. *Matrix Biology* 29 (8): 678–89. https://doi.org/10.1016/j.matbio.2010.08.009.

Kapacee, Zoher, Susan H. Richardson, Yinhui Lu, Tobias Starborg, David F. Holmes, Keith Baar, and Karl E. Kadler. 2008. 'Tension Is Required for Fibripositor Formation'. *Matrix Biology* 27 (4): 371–75. https://doi.org/10.1016/j.matbio.2007.11.006.

Kapacee, Zoher, Ching Yan Chloé Yeung, Yinhui Lu, David Crabtree, David F. Holmes, and Karl E. Kadler. 2010. 'Synthesis of Embryonic Tendon-like Tissue by Human Marrow Stromal/Mesenchymal Stem Cells Requires a Three-Dimensional Environment and Transforming Growth Factor B3'. *Matrix Biology* 29 (8): 668–77. https://doi.org/10.1016/j.matbio.2010.08.005.

Kokai, Lauren E., Kacey Marra, and J. Peter Rubin. 2014. 'Adipose Stem Cells: Biology and Clinical Applications for Tissue Repair and Regeneration'. *Translational Research* 163 (4): 399–408. https://doi.org/10.1016/j.trsl.2013.11.009.

Kuo, Catherine K., and Rocky S. Tuan. 2008. 'Mechanoactive Tenogenic Differentiation of Human Mesenchymal Stem Cells'. *Tissue Engineering - Part A.* 14 (10): 1615–27. https://doi.org/10.1089/ten.tea.2006.0415.

Kyriakides, Themis R., Yu Hong Zhu, Lynne T. Smith, Steven D. Bain, Zhantao Yang, Ming T. Lin, Keith G. Danielson, et al. 1998. 'Mice That Lack Thrombospondin 2 Display Connective Tissue Abnormalities That Are Associated with Disordered Collagen Fibrillogenesis, an Increased Vascular Density, and a Bleeding Diathesis'. *Journal of Cell Biology* 140 (2): 419–30. https://doi.org/10.1083/jcb.140.2.419.

Li, Haiyin, Antonion Korcari, David Ciufo, Christopher L. Mendias, Scott A. Rodeo, Mark R. Buckley, Alayna E. Loiselle, Geoffrey S. Pitt, and Chike Cao. 2023. 'Increased Ca2+ Signaling through CaV 1.2 Induces Tendon Hypertrophy with Increased Collagen Fibrillogenesis and Biomechanical Properties'. *FASEB Journal : Official Publication of the Federation of American Societies for Experimental Biology* 37 (7): e23007. https://doi.org/10.1096/fj.202300607R.

Liu, Wenjin, Spencer S. Watson, Yu Lan, Douglas R. Keene, Catherine E. Ovitt, Han Liu, Ronen Schweitzer, and Rulang Jiang. 2010. 'The Atypical Homeodomain Transcription Factor Mohawk Controls Tendon Morphogenesis'. *Molecular and Cellular Biology* 30 (20): 4797–4807. https://doi.org/10.1128/mcb.00207-10.

Livak, Kenneth J., and Thomas D. Schmittgen. 2001. 'Analysis of Relative Gene Expression Data Using Real-Time Quantitative PCR and the 2−ΔΔCT Method'. *Methods* 25 (4): 402–8. https://doi.org/10.1006/meth.2001.1262.

Marturano, Joseph E, Jeffrey D Arena, Zachary A Schiller, Irene Georgakoudi, and Catherine K Kuo. 2013. 'Characterization of Mechanical and Biochemical Properties of Developing Embryonic Tendon'. *Proceedings of the National Academy of Sciences* 110 (16): 6370 LP – 6375. https://doi.org/10.1073/pnas.1300135110.

Micheli, Andrea J. de, Jacob B. Swanson, Nathaniel P. Disser, Leandro M. Martinez, Nicholas R. Walker, David J. Oliver, Benjamin D. Cosgrove, and Christopher L. Mendias. 2020. 'Single-Cell Transcriptomic Analysis Identifies Extensive Heterogeneity in the Cellular Composition of Mouse Achilles Tendons'. *American Journal of Physiology - Cell Physiology* 319 (5): C885–94. https://doi.org/10.1152/ajpcell.00372.2020.

Miroshnikova, Yekaterina A., and Sara A. Wickström. 2022. 'Mechanical Forces in Nuclear Organization'. *Cold Spring Harbor Perspectives in Medicine* 14 (1). https://doi.org/10.1101/cshperspect.a039685.

Mousavizadeh, Rouhollah, Charlie M. Waugh, Erin DeBruin, Robert G. McCormack, Vincent Duronio, and Alex Scott. 2023. 'Exposure to OxLDL Impairs TGF-β Activity in Human Tendon Cells'. *BMC Musculoskeletal Disorders* 24 (1). https://doi.org/10.1186/s12891-023-06308-x.

Murchison, Nicholas D, Brian A Price, David A Conner, Douglas R Keene, Eric N Olson, Clifford J Tabin, and Ronen Schweitzer. 2007. 'Regulation of Tendon Differentiation by Scleraxis Distinguishes Force-Transmitting Tendons from Muscle-Anchoring Tendons'. *Development* 134 (14): 2697 LP – 2708. https://doi.org/10.1242/dev.001933.

Nguyen, Phong K., Kaitlyn Hall, Iverson Holt, and Catherine K. Kuo. 2023. 'Recombinant Lysyl Oxidase Effects on Embryonic Tendon Cell Phenotype and Behavior'. *Journal of Orthopaedic Research* 41 (10): 2175–85. https://doi.org/10.1002/jor.25655.

Okamoto, Osamu, and Sakuhei Fujiwara. 2006. 'Dermatopontin, a Novel Player in the Biology of the Extracellular Matrix'. *Connective Tissue Research* 47 (4): 177–89. https://doi.org/10.1080/03008200600846564.

Omoto, Takenori, Dilimulati Yimiti, Yohei Sanada, Minoru Toriyama, Chenyang Ding, Yuta Hayashi, Yasunari Ikuta, et al. 2022. 'Tendon-Specific Dicer Deficient Mice Exhibit Hypoplastic Tendon Through the Downregulation of Tendon-Related Genes and MicroRNAs'. *Frontiers in Cell and Developmental Biology* 10 (June): 1–14. https://doi.org/10.3389/fcell.2022.898428.

Otabe, Koji, Hiroyuki Nakahara, Akihiko Hasegawa, Tetsuya Matsukawa, Fumiaki Ayabe, Naoko Onizuka, Masafumi Inui, et al. 2015. 'Transcription Factor Mohawk Controls Tenogenic Differentiation of Bone Marrow Mesenchymal Stem Cells in Vitro and in Vivo'. *Journal of Orthopaedic Research* 33 (1): 1–8. https://doi.org/10.1002/jor.22750.

Pan, Te Cheng, Rui Zhu Zhang, Dessislava Markova, Machiko Arita, Yejia Zhang, Sasha Bogdanovich, Tejvir S. Khurana, Carsten G. Bönnemann, David E. Birk, and Mon Li Chu. 2013. 'COL6A3 Protein Deficiency in Mice Leads to Muscle and Tendon Defects Similar to Human Collagen VI Congenital Muscular Dystrophy'. *Journal of Biological Chemistry* 288 (20): 14320–31. https://doi.org/10.1074/jbc.M112.433078.

Park, Hyeree, Showan N. Nazhat, and Derek H. Rosenzweig. 2022. 'Mechanical Activation Drives Tenogenic Differentiation of Human Mesenchymal Stem Cells in Aligned Dense Collagen Hydrogels'. *Biomaterials* 286 (May): 121606. https://doi.org/10.1016/j.biomaterials.2022.121606.

Pechanec, Monica Y., Tannah N. Boyd, Keith Baar, and Michael J. Mienaltowski. 2020. 'Adding Exogenous Biglycan or Decorin Improves Tendon Formation for Equine Peritenon and Tendon Proper Cells in Vitro'. *BMC Musculoskeletal Disorders* 21 (1). https://doi.org/10.1186/s12891-020-03650-2.

Peltonen, Jussi, Neil J. Cronin, Lauri Stenroth, Taija Finni, and Janne Avela. 2013. 'Viscoelastic Properties of the Achilles Tendon in Vivo'. *SpringerPlus* 2 (1): 1–8. https://doi.org/10.1186/2193-1801-2-212.

Pentzold, Stefan, and Britt Wildemann. 2022. 'Mechanical Overload Decreases Tenogenic Differentiation Compared to Physiological Load in Bioartificial Tendons'. *Journal of Biological Engineering* 16 (1): 1–10. https://doi.org/10.1186/s13036-022-00283-y.

Réty, Stéphane, Dirk Osterloh, Jean-Philippe Arié, Sébastien Tabaries, Joachim Seeman, Françoise Russo-Marie, Volker Gerke, and Anita Lewit-Bentley. 2000. 'Structural Basis of the Ca 2+-Dependent Association between S100C (S100A11) and Its Target, the N-Terminal Part of Annexin I'.

Saraswathibhatla, Aashrith, Dhiraj Indana, and Ovijit Chaudhuri. 2023. 'Cell-Extracellular Matrix Mechanotransduction in 3D HHS Public Access'. *Nat Rev Mol Cell Biol* 24 (7): 495–516. https://doi.org/10.1038/s415XX-XXX-XXXX-X.

Schulz Torres, Donna, Toby M. Freyman, Ioannis V. Yannas, and Myron Spector. 2000. 'Tendon Cell Contraction of Collagen-GAG Matrices in Vitro: Effect of Cross-Linking'. *Biomaterials* 21 (15): 1607–19. https://doi.org/10.1016/S0142-9612(00)00051-X.

Schweitzer, R., J. H. Chyung, L. C. Murtaugh, A. E. Brent, V. Rosen, E. N. Olson, A. Lassar, and C. J. Tabin. 2001. 'Analysis of the Tendon Cell Fate Using Scleraxis, a Specific Marker for Tendons and Ligaments'. *Development* 128 (19): 3855–66. https://doi.org/10.1242/dev.128.19.3855.

Scott, A., P. Danielson, T. Abraham, G. Fong, A. V. Sampaio, and T. M. Underhill. 2011. 'Mechanical Force Modulates Scleraxis Expression in Bioartificial Tendons'. *Journal of Musculoskeletal Neuronal Interactions* 11 (2): 124–32.

Shukunami, Chisa, Aki Takimoto, Yuriko Nishizaki, Yuki Yoshimoto, Seima Tanaka, Shigenori Miura, Hitomi Watanabe, et al. 2018. 'Scleraxis Is a Transcriptional Activator That Regulates the Expression of Tenomodulin, a Marker of Mature Tenocytes and Ligamentocytes'. *Scientific Reports* 8 (1): 3155. https://doi.org/10.1038/s41598-018-21194-3.

Shukunami, Chisa, Aki Takimoto, Miwa Oro, and Yuji Hiraki. 2006. 'Scleraxis Positively Regulates the Expression of Tenomodulin, a Differentiation Marker of Tenocytes'. *Developmental Biology* 298 (1): 234–47. https://doi.org/10.1016/j.ydbio.2006.06.036.

Steffen, Danielle, Michael Mienaltowski, and Keith Baar. 2023. 'Spatial Gene Expression in the Adult Rat Patellar Tendon'. *Matrix Biology Plus* 19–20 (December). https://doi.org/10.1016/j.mbplus.2023.100138.

Vaughan, Melville B., Gang Xu, Tracy L. Morris, Pratiksha Kshetri, and Jing X. Herwig. 2019. 'Predictable Fibroblast Tension Generation by Measuring Compaction of Anchored Collagen Matrices Using Microscopy and Optical Coherence Tomography'. *Cell Adhesion and Migration* 13 (1): 303–14. https://doi.org/10.1080/19336918.2019.1644855.

Waldner, Matthias, Wensheng Zhang, Isaac B. James, Kassandra Allbright, Emmanuelle Havis, Jacqueline M. Bliley, Aurora Almadori, et al. 2018. 'Characteristics and Immunomodulating Functions of Adipose-Derived and Bone Marrow-Derived Mesenchymal Stem Cells across Defined Human Leukocyte Antigen Barriers'. *Frontiers in Immunology* 9 (JUL). https://doi.org/10.3389/fimmu.2018.01642.

Wang, Jia, Zhiyong Tan, Yinglong Huang, Charles Li, Peiqin Zhan, Haifeng Wang, and Haihao Li. 2024. 'Integrating Single-Cell RNA-Seq to Identify Fibroblast-Based Molecular Subtypes for Predicting Prognosis and Therapeutic Response in Bladder Cancer'. *AGING 2024*. Vol. 16. www.aging-us.comwww.aging-us.com.

Wang, Tao, Peilin Chen, Monica Zheng, Allan Wang, David Lloyd, Toby Leys, Qiujian Zheng, and Ming H. Zheng. 2018. 'In Vitro Loading Models for Tendon Mechanobiology'. *Journal of Orthopaedic Research* 36 (2): 566–75. https://doi.org/10.1002/jor.23752.

Yan, Zhibin, Xurui Cheng, Tao Wang, Xiangyu Hong, Gang Shao, and Caiyun Fu. 2022. 'Therapeutic Potential for Targeting Annexin A1 in Fibrotic Diseases'. *Genes and Diseases*. Chongqing University. https://doi.org/10.1016/j.gendis.2022.05.038.

Yang, Guang, Benjamin B. Rothrauff, Hang Lin, Riccardo Gottardi, Peter G. Alexander, and Rocky S. Tuan. 2013. 'Enhancement of Tenogenic Differentiation of Human Adipose Stem Cells by Tendon-Derived Extracellular Matrix'. *Biomaterials* 34 (37): 9295–9306. https://doi.org/10.1016/j.biomaterials.2013.08.054.

Yeung, Ching Yan Chloé, Leo A.H. Zeef, Chloe Lallyett, Yinhui Lu, Elizabeth G. Canty-Laird, and Karl E. Kadler. 2015. 'Chick Tendon Fibroblast Transcriptome and Shape Depend on Whether the Cell Has Made Its Own Collagen Matrix'. *Scientific Reports* 5 (September). https://doi.org/10.1038/srep13555.

Zhang, Guiyun, Yoichi Ezura, Inna Chervoneva, Paul S. Robinson, David P. Beason, Ehren T. Carine, Louis J. Soslowsky, Renato V. Iozzo, and David E. Birk. 2006. 'Decorin Regulates Assembly of Collagen Fibrils and Acquisition of Biomechanical Properties during Tendon Development'. *Journal of Cellular Biochemistry* 98 (6): 1436–49. https://doi.org/10.1002/jcb.20776.

Zhao, Jiarui, Chuanqing Jing, Rui Fan, and Wei Zhang. 2024. 'Prognostic Model of Fibroblasts in Idiopathic Pulmonary Fibrosis by Combined Bulk and Single-Cell RNA-Sequencing'. *Heliyon* 10 (14). https://doi.org/10.1016/j.heliyon.2024.e34519.

Zuk, Patricia. 2013. 'Adipose-Derived Stem Cells in Tissue Regeneration: A Review'. *International Scholarly Research Notices* 2013 (1): e713959. https://doi.org/10.1155/2013/713959.

Figure Legends

Figure 1: Generation of 3D-hASC constructs using a Flexcell bioreactor. A) Human adipose stromal cells are isolated from lipoaspirates and amplified before seeding. The cells are embedded in a 3.5% collagen hydrogel and deposited between the two anchor points. The polymerization is performed by maintaining the vacuum and at 37°C for 2 hours. The vacuum is then broken and the 3D-hASC constructs are kept in the incubator for 48 hours before starting the experiments. Scale bar 100µm. B) 3D-hASC constructs were cultured for 21 days and C) Diameters were measured from constructs at Day 0 (n=11), Day 7 (n=15), Day 14 (n=14) and Day 21 (n=19). Each color represents a set of experiments. 4 independent experiments were performed with 3<n<8 biological replicates for each experiment. The p-values were obtained using the Mann-Whitney test. Asterisks * indicate the p-values of 3D-hASCs construct diameter compared to each following stage, ****P<0.001. Scale bars 500µm. D) 3D-hASC construct total cell number was counted at Day 0 (n=9), Day 7 (n=9), Day 14 (n=9) and Day 21 (n=9). Each color represents a set of experiments. 3 independent experiments were performed with n=3 biological replicates for each experiment. The p-values were obtained using the Mann-Whitney test. Asterisks * indicate the p-values of 3D-hASCs construct cell number compared to each following stage, ** P<0.01, ****P<0.0001. E) Longitudinal sections of 3D-hASC constructs were performed at Day 4 and stained with DAPI/Phalloidin to visualize cellular and nuclear shape. Scale bars: 50 µm. F) Longitudinal sections of 3D-hASC constructs were performed on Day 0, Day 2, Day 4, Day 7, Day 14 and Day 21. The angles of 15 cells were measured on a minimum of 3 constructs per time point and compared to the axis of tension. Each dot represents the mean of 15 values per 3D-hASC construct. Asterisks * indicate the p-values of 3D-hASCs construct cell number compared to each following stage, * P<0.05, **P<0.01. G) After 0, 2, 4, 7, 14 and 21 Days of culture, 3D-hASC constructs were used for mRNA purification. mRNA expression levels of *COL1A1* were analysed by RT-qPCR. H) 3D-hASC constructs at Day 4 were transversally cryo-sectioned. 12 µm sections were hybridized with the DIG-labeled antisense probes for *COL1A1*. Scale bar: 250µm. I) 3D-hASC constructs at Day 4 Day 0, Day 7, Day 14 and Day 21 were transversally cryo-sectioned. 12 µm sections were hybridized with the DIG-labeled antisense probes for *COL1A1*. Scale bars: 50µm.

Figure 2: 3D-hASC constructs express tendon genes. A) After 0, 2, 4, 7, 14 and 21 Days of culture, 3D-hASC constructs were used for mRNA purification. mRNA expression levels of *SCX* were analysed by RT-qPCR. B) 3D-hASC constructs at Day 0, Day 7, Day 14 and Day 21 were transversally cryo-sectioned. 12 µm sections were hybridized with the DIG-labeled antisense probes for *SCX*. Scale bars: 50µm. After 0, 2, 4, 7, 14 and 21 Days of culture, 3D-hASC constructs were used for mRNA purification. mRNA samples were analysed by RT-qPCR for C) *MKX* D) *TNMD* and E) *THBS2*. F) 3D-hASC constructs at Day 0, Day 7, Day 14 and Day 21 were transversally cryo-sectioned. 12 µm sections were hybridized with the DIG-labeled antisense probes for *THBS2.* Scale bars 50µm. mRNA expression levels of G) *TM4FS1*, H) *ANXA1*, I) *S100A10*, J) *COL2A1* were analysed by RT-qPCR. Transcripts are shown relative to the level of *YWHAZ* transcripts. The relative mRNA levels were calculated using the $2^{\wedge-\Delta\Delta Ct}$ method, with control being normalized to 1. Each color represents a set of experiments. 8 independent experiments were performed with 14 < n < 29 3D-hASCs construct generated for each step (n=29 at Day 0, n=19 at Day 2, n=18 at Day 4, n=25 at Day 7, n=17 at Day 14 and n=16 at Day 21). The C_T values shown for tendon genes and *YWHAZ* represent the average of all C_T values obtained for each time point. Error bars represent the mean + standard deviations. The p-values were obtained using the Mann-Whitney test. Asterisks * indicate the p-values of

857 gene expression levels in 3D-hASC constructs compared to the first Day of gene detection
858 *P<0.05, **P<0.01, *** P<0.001, **** P<0.0001.
859
860 **Figure 3: 3D-hASC construct Young's modulus increased along time.** A) 3D-hASC
861 constructs are fixed on a 3D-printed support maintained in agarose gel. B) 3D-hASC constructs
862 are placed in an appropriate channel according to their diameter and fixed using dissection pins
863 inserted into the anchor stems and agarose. C) The one-piece optical probe of the nanoindenter
864 is composed of an optical fiber, a cantilever and a spherical tip. After an approach phase, the
865 tip touches the sample and indent it. The cantilever bending is detected by the optical fiber.
866 D) Force as a function of cantilever base displacement for a typical indentation. Inset:
867 Cantilever base displacement is applied at constant rate of 10µm.s-1. E) Force as a function of
868 indentation for a typical indentation curve. Hertz contact fit (red) is applied over a 1 µm
869 indentation. F) Cumulative distribution function (CDF) of effective Young's modulus along
870 culture time in 3D-hASCs. The 0.5 CDF value corresponds to the median Young's modulus
871 value. Indentation experiments were performed at Day 0 (n=17), Day 7 (n=17), Day 14 (n=13)
872 and Day 21 (n=14). 5 independent experiments were performed with 3<n<8 biological
873 replicates for each experiment. G) Cumulative distribution function (CDF) of effective Young's
874 modulus along culture time in 3D-constructs without cells. Indentation experiments were
875 performed at Day 0 (n=8), Day 7 (n=6), Day 14 (n=6) and Day 21 (n=12). 2 independent
876 experiments were performed with 3<n<6 biological replicates for each experiment.
877
878 **Figure 4: Extra-cellular matrix gene expression was highly increased during 3D-hASC**
879 **construct development.** After 0, 2, 4, 7, 14 and 21 Days of culture, 3D-hASC constructs were
880 used for mRNA purification. mRNA expression levels of tendon-associated collagens A)
881 *COL6A3*, B) *COL14A1* and extracellular matrix protein coding genes C) *DCN*, D) *POSTN,* E)
882 *DPT* and F) *LOX* were analysed by RT-qPCR. Transcripts are shown relative to the level of
883 *YWHAZ* transcripts. The relative mRNA levels were calculated using the $2^{\wedge-\Delta\Delta Ct}$ method, with
884 control being normalized to 1. Each color represents a set of experiments. 8 independent
885 experiments were performed with 14 < n < 29 3D-hASCs construct generated for each step
886 (n=29 at Day 0, n=19 at Day 2, n=18 at Day 4, n=25 at Day 7, n=17 at Day 14 and n=16 at Day
887 21). The C_T values shown for tendon genes and *YWHAZ* represent the average of all C_T values
888 obtained for each time point. Error bars represent the mean + standard deviations. The p-values
889 were obtained using the Mann-Whitney test. Asterisks * indicate the p-values of gene
890 expression levels in 3D-hASC constructs compared to the first Day of gene detection *P<0.05,
891 **P<0.01, *** P<0.001, **** P<0.0001.
892
893 **Figure 5: Viscoelastic properties of human 3D-hASC constructs change over the course**
894 **of the culture.** A) Schematic of a force relaxation experiment. In open loop, the base of the
895 cantilever is fixed while relaxation takes place. B) Typical curve showing force as a function
896 of indentation during loading, relaxation and unloading phase. Inset: Indentation as a function
897 of time. C) Force as a function of cantilever base displacement for a typical indentation. Inset:
898 Cantilever base displacement is applied at constant rate of 10µm.s-1. D) Force as a function
899 time. Force peaks at a value Fmax and reaches is close to a plateau after 10s of relaxation.
900 Frelax is defined as the force at this instant. E) Percentage of stress relaxation ((Fmax – Ft=10
901 sec) / Fmax)) x100 during the first 10 seconds of relaxation, after different periods of cell
902 culture. For 3D-no cell constructs without cells, each dot represents the mean of five
903 measurements performed on one construct. Indentation experiments were performed at Day 0
904 (n=8), Day 7 (n=6), Day 14 (n=6) and Day 21 (n=12). Each color represents a set of
905 experiments. 2 independent experiments were performed with 3<n<6 biological replicates for
906 each experiment. For 3D-hASC constructs, indentation experiments were performed at Day 0

907 (n=17), Day 7 (n=17), Day 14 (n=13) and Day 21 (n=14). Each color represents a set of
908 experiments. 5 independent experiments were performed with 3<n<8 biological replicates for
909 each experiment. The p-values were obtained using the Mann-Whitney test. Asterisks *
910 indicates the p-value of 3D-hASCs construct relaxation compared to each following stage;
911 *P<0.05; @ indicates the p-value of 3D-no cell construct relaxation compared to each following
912 stage, @P<0.05; # indicates the p-value of in 3D-no cell constructs compared to 3D-hASC
913 constructs, ###P<0.001, ####P<0.0001.
914
915 **Figure 6: Cellular organization in 3D engineered 3D-hASCs.** A) 3D-hASCs transverse
916 section representation. B) Transverse sections of 3D-hASC constructs were performed on Day
917 0, Day 2, Day 4, Day 7, Day 14 and Day 21 of culture and stained with DAPI/Phalloidin to
918 visualize cell organization within the 3D-hASC constructs. From Day 2, 3D-hASC constructs
919 are composed of two cell populations, one at the centre and the other at the periphery, forming
920 a ring. D) Cell density was counted at the centre and the ring of 3D-hASC constructs at Day 0
921 (n=18), Day 2 (n=12), Day 4 (n=10), Day 7 (n=15), Day 14 (n=12) and Day 21 (n=9). The p-
922 values were obtained using the Mann-Whitney test compared to each following stage. Asterisks
923 * indicate the p-values of cell number at the centre, *** P <0.001, **** P<0.0001; # indicate
924 the p-values of cell number at the ring, #### P <0.0001; Scale bars 100µm.
925
926
927
928
929
930
931

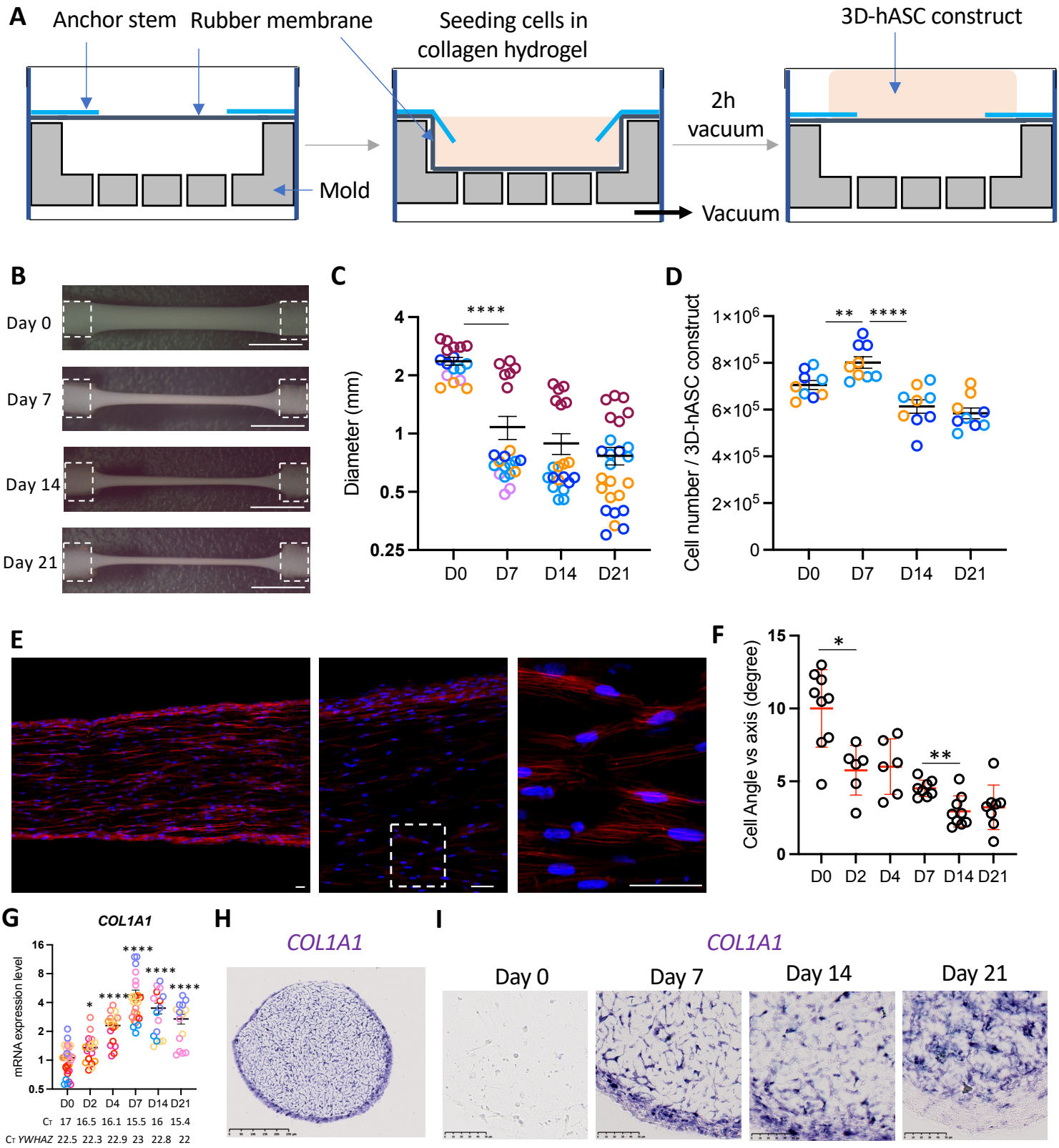
A
Anchor stem
Rubber membrane
Seeding cells in collagen hydrogel
3D-hASC construct
2h vacuum
Mold
Vacuum
B
Day 0
Day 7
Day 14
Day 21
C
Diameter (mm)
D0 D7 D14 D21
D
Cell number / 3D-hASC construct
D0 D7 D14 D21
E
F
Cell Angle vs axis (degree)
D0 D2 D4 D7 D14 D21
G
COL1A1
mRNA expression level
D0 D2 D4 D7 D14 D21
CT 17 16.5 16.1 15.5 16 15.4
CT YWHAZ 22.5 22.3 22.9 23 22.8 22
H
COL1A1
I
COL1A1
Day 0
Day 7
Day 14
Day 21

Figure 1

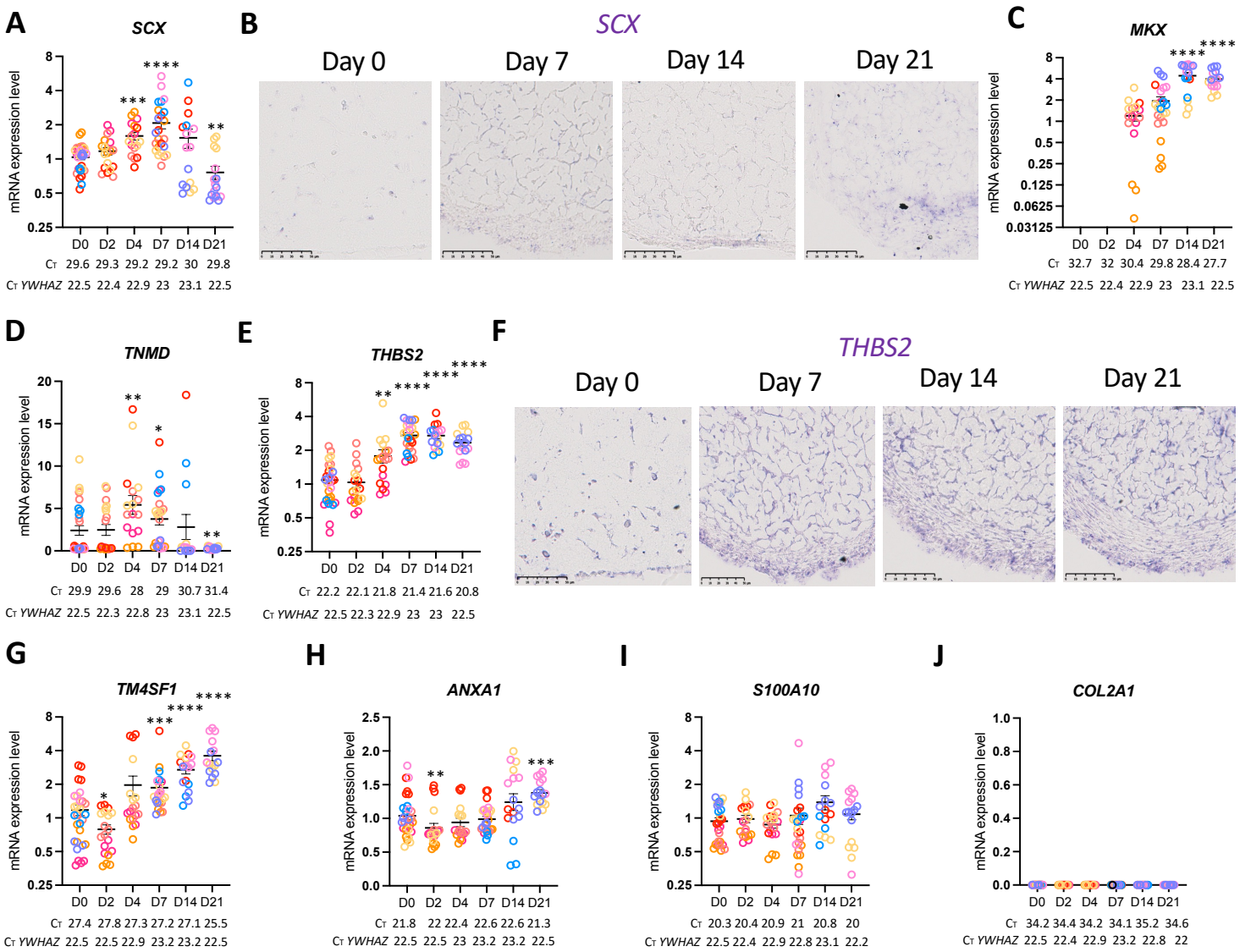
A
SCX
mRNA expression level
D0 D2 D4 D7 D14 D21
CT 29.6 29.3 29.2 29.2 30 29.8
CT YWHAZ 22.5 22.4 22.9 23 23.1 22.5
B
SCX
Day 0
Day 7
Day 14
Day 21
C
MKX
mRNA expression level
D0 D2 D4 D7 D14 D21
CT 32.7 32 30.4 29.8 28.4 27.7
CT YWHAZ 22.5 22.4 22.9 23 23.1 22.5
D
TNMD
mRNA expression level
D0 D2 D4 D7 D14 D21
CT 29.9 29.6 28 29 30.7 31.4
CT YWHAZ 22.5 22.3 22.8 23 23.1 22.5
E
THBS2
mRNA expression level
D0 D2 D4 D7 D14 D21
CT 22.2 22.1 21.8 21.4 21.6 20.8
CT YWHAZ 22.5 22.3 22.9 23 23 22.5
F
THBS2
Day 0
Day 7
Day 14
Day 21
G
TM4SF1
mRNA expression level
D0 D2 D4 D7 D14 D21
CT 27.4 27.8 27.3 27.2 27.1 25.5
CT YWHAZ 22.5 22.5 22.9 23.2 23.2 22.5
H
ANXA1
mRNA expression level
D0 D2 D4 D7 D14 D21
CT 21.8 22 22.4 22.6 22.6 21.3
CT YWHAZ 22.5 22.5 23 23.2 23.2 22.5
I
S100A10
mRNA expression level
D0 D2 D4 D7 D14 D21
CT 20.3 20.4 20.9 21 20.8 20
CT YWHAZ 22.5 22.4 22.9 22.8 23.1 22.2
J
COL2A1
mRNA expression level
D0 D2 D4 D7 D14 D21
CT 34.2 34.4 34.2 34.1 35.2 34.6
CT YWHAZ 22.5 22.4 22.9 23.2 22.8 22

Figure 2

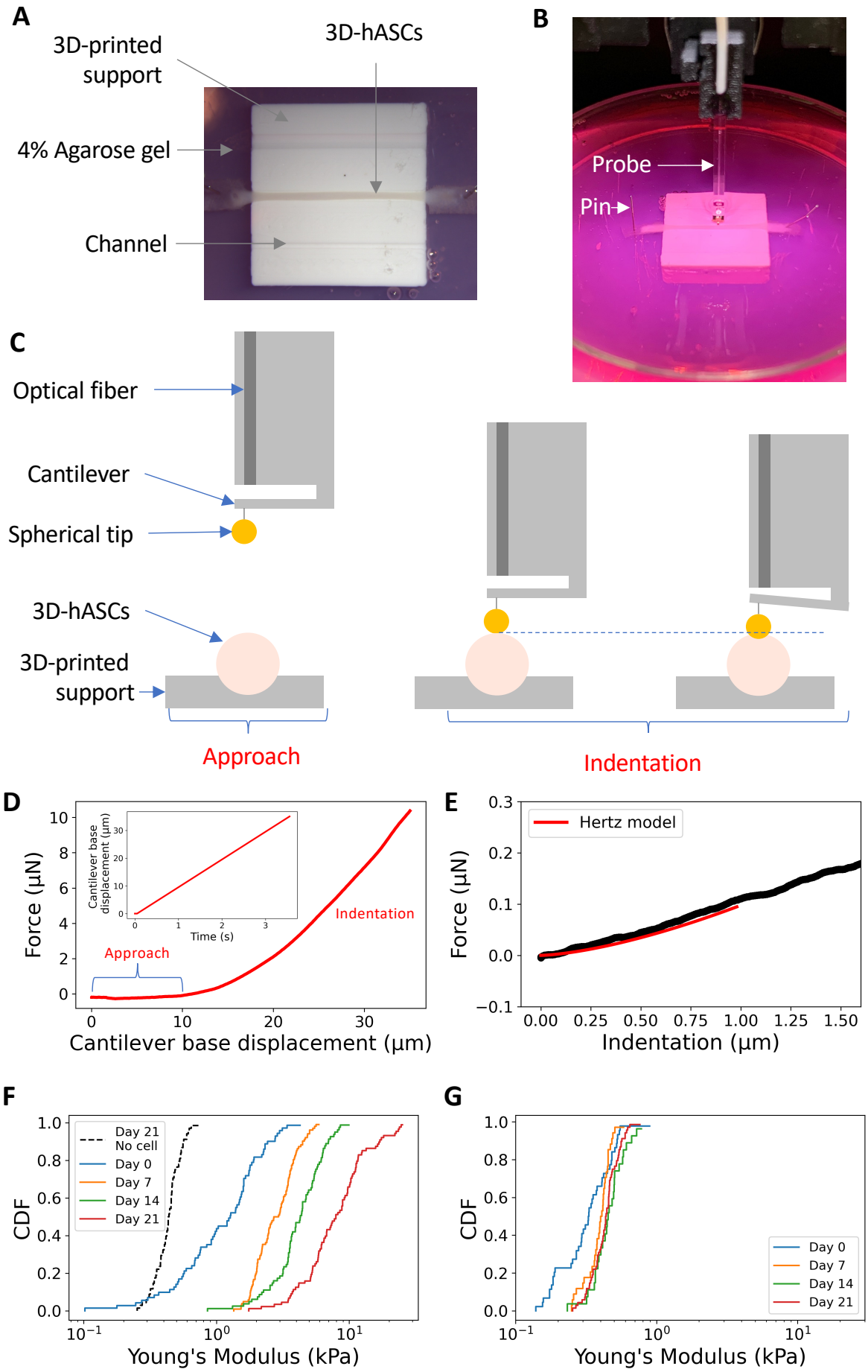
A
3D-printed support
3D-hASCs
4% Agarose gel
Channel
B
Probe
Pin
C
Optical fiber
Cantilever
Spherical tip
3D-hASCs
3D-printed support
Approach
Indentation
D
Force (μN)
Cantilever base displacement (μm)
Cantilever base displacement (μm)
Time (s)
Approach
Indentation
E
Hertz model
Force (μN)
Indentation (μm)
F
CDF
Day 21 No cell
Day 0
Day 7
Day 14
Day 21
Young's Modulus (kPa)
G
CDF
Day 0
Day 7
Day 14
Day 21
Young's Modulus (kPa)

Figure 3

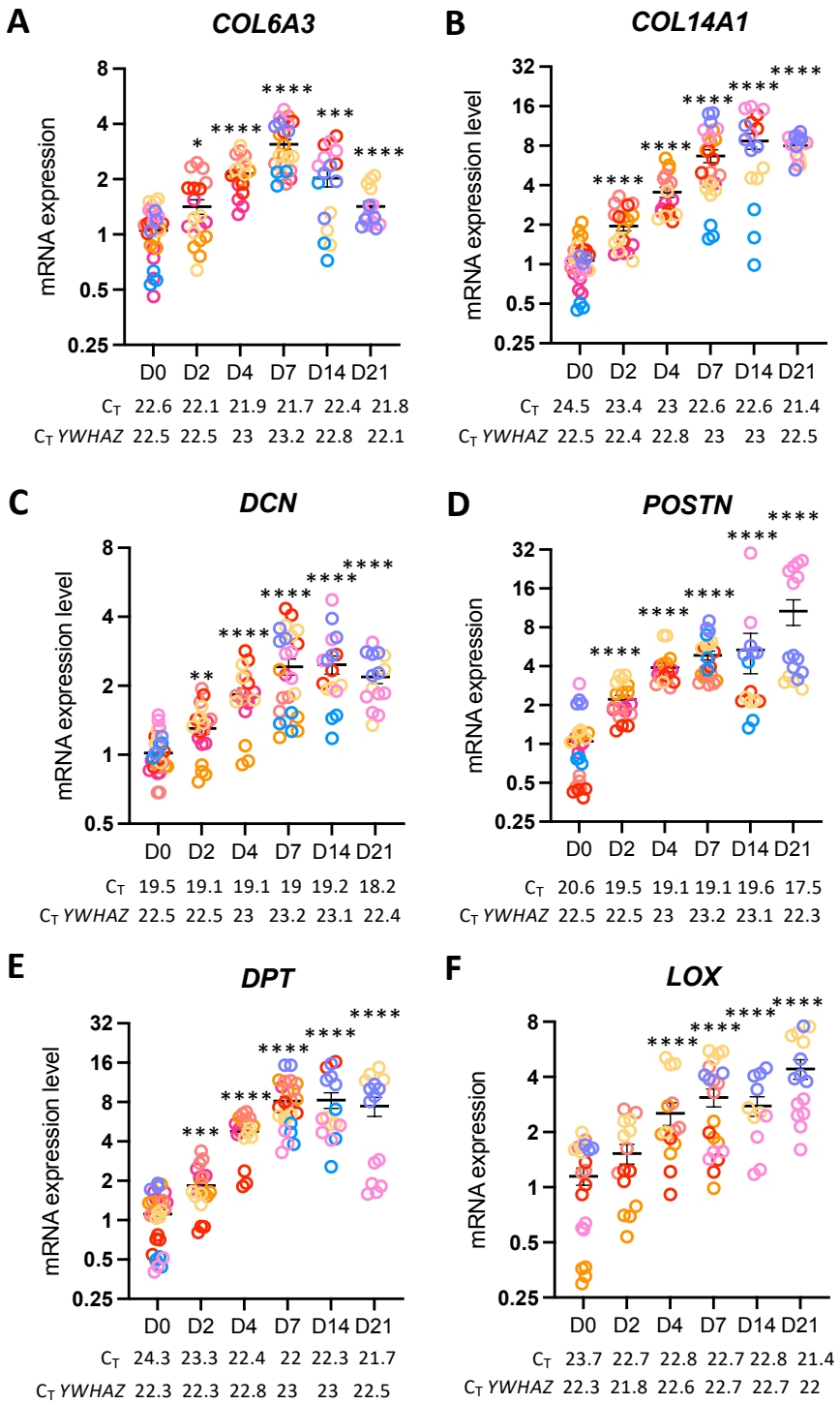
A
COL6A3
mRNA expression
8
4
2
1
0.5
0.25
D0 D2 D4 D7 D14 D21
CT 22.6 22.1 21.9 21.7 22.4 21.8
CT YWHAZ 22.5 22.5 23 23.2 22.8 22.1
B
COL14A1
mRNA expression level
32
16
8
4
2
1
0.5
0.25
D0 D2 D4 D7 D14 D21
CT 24.5 23.4 23 22.6 22.6 21.4
CT YWHAZ 22.5 22.4 22.8 23 23 22.5
C
DCN
mRNA expression level
8
4
2
1
0.5
D0 D2 D4 D7 D14 D21
CT 19.5 19.1 19.1 19 19.2 18.2
CT YWHAZ 22.5 22.5 23 23.2 23.1 22.4
D
POSTN
mRNA expression
32
16
8
4
2
1
0.5
0.25
D0 D2 D4 D7 D14 D21
CT 20.6 19.5 19.1 19.1 19.6 17.5
CT YWHAZ 22.5 22.5 23 23.2 23.1 22.3
E
DPT
mRNA expression level
32
16
8
4
2
1
0.5
0.25
D0 D2 D4 D7 D14 D21
CT 24.3 23.3 22.4 22 22.3 21.7
CT YWHAZ 22.3 22.3 22.8 23 23 22.5
F
LOX
mRNA expression
8
4
2
1
0.5
0.25
D0 D2 D4 D7 D14 D21
CT 23.7 22.7 22.8 22.7 22.8 21.4
CT YWHAZ 22.3 21.8 22.6 22.7 22.7 22

Figure 4

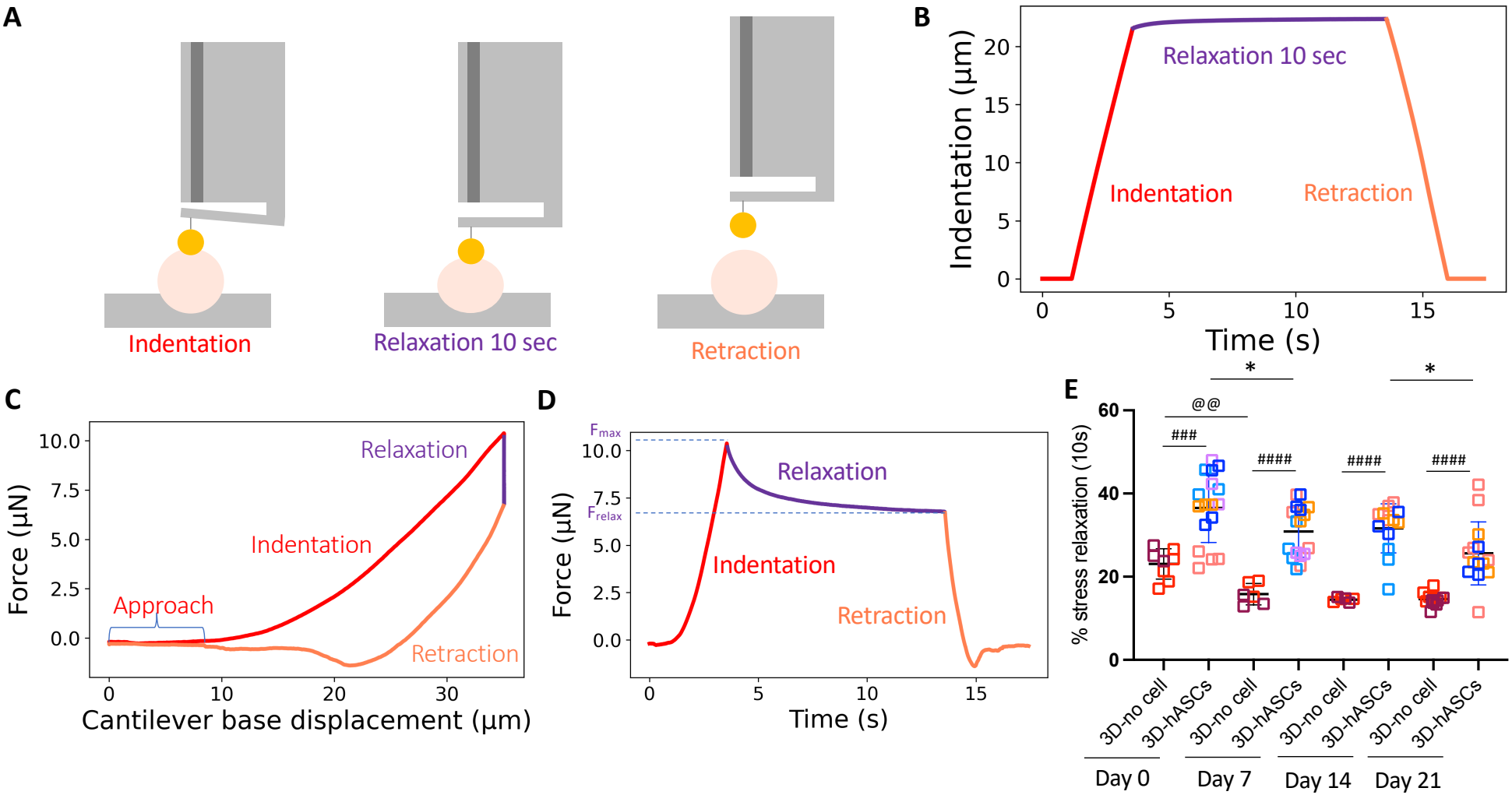
A
Indentation
Relaxation 10 sec
Retraction
B
Indentation (µm)
Time (s)
Relaxation 10 sec
Indentation
Retraction
C
Force (µN)
Cantilever base displacement (µm)
Approach
Indentation
Relaxation
Retraction
D
Force (µN)
Time (s)
Fmax
Frelax
Relaxation
Indentation
Retraction
E
% stress relaxation (10s)
@@
###
####
3D-no cell
3D-hASCs
Day 0
Day 7
Day 14
Day 21

Figure 5

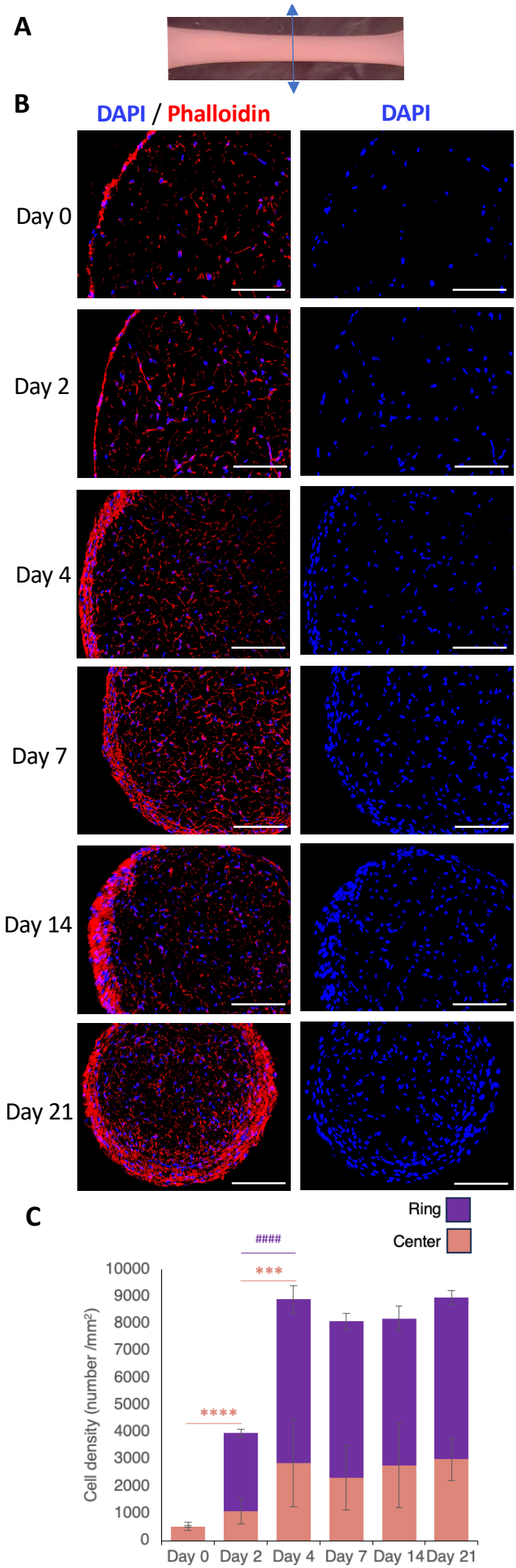
A
B
DAPI / Phalloidin
DAPI
Day 0
Day 2
Day 4
Day 7
Day 14
Day 21
C
Ring
Center
####
***
****
Cell density (number /mm²)
10000
9000
8000
7000
6000
5000
4000
3000
2000
1000
0
Day 0
Day 2
Day 4
Day 7
Day 14
Day 21

Figure 6